IEEE Access
Multidisciplinary | Rapid Review | Open Access Journal

SPECIAL SECTION ON DEEP LEARNING ALGORITHMS FOR INTERNET OF MEDICAL THINGS

Received April 10, 2020, accepted May 2, 2020, date of publication May 11, 2020, date of current version June 15, 2020.

Digital Object Identifier 10.1109/ACCESS.2020.2993937

Diabetic Retinopathy Detection Using Prognosis of Microaneurysm and Early Diagnosis System for Non-Proliferative Diabetic Retinopathy Based on Deep Learning Algorithms

LIFENG QIAO[1], YING ZHU[2], AND HUI ZHOU[2]

[1]Department of Ophthalmology, Sichuan Academy of Medical Sciences and Sichuan Provincial People's Hospital, Chengdu 610072, China
[2]Department of Endocrinology, Sichuan Academy of Medical Sciences and Sichuan Provincial People's Hospital, Chengdu 610072, China

Corresponding author: Hui Zhou (zhouhuinf@med.uestc.edu.cn)

ABSTRACT Predicting the presence of Microaneurysms in the fundus images and the identification of diabetic retinopathy in early-stage has always been a major challenge for decades. Diabetic Retinopathy (DR) is affected by prolonged high blood glucose level which leads to microvascular complications and irreversible vision loss. Microaneurysms formation and macular edema in the retinal is the initial sign of DR and diagnosis at the right time can reduce the risk of non proliferated diabetic retinopathy. The rapid improvement of deep learning makes it gradually become an efficient technique to provide an interesting solution for medical image analysis problems. The proposed system analysis the presence of microaneurysm in fundus image using convolutional neural network algorithms that embeds deep learning as a core component accelerated with GPU(Graphics Processing Unit) which will perform medical image detection and segmentation with high-performance and low-latency inference. The semantic segmentation algorithm is utilized to classify the fundus picture as normal or infected. Semantic segmentation divides the image pixels based on their common semantic to identify the feature of microaneurysm. This provides an automated system that will assist ophthalmologists to grade the fundus images as early NPDR, moderate NPDR, and severe NPDR. The Prognosis of Microaneurysm and early diagnosis system for non - proliferative diabetic retinopathy system has been proposed that is capable to train effectively a deep convolution neural network for semantic segmentation of fundus images which can increase the efficiency and accuracy of NPDR (non proliferated diabetic retinopathy) prediction.

INDEX TERMS Microaneurysm, diabetic retinopathy, deep convolution neural network, semantic segmentation, non proliferated diabetic retinopathy.

I. INTRODUCTION

The main causing of visual loss in the world is diabetic retinopathy. In the initial stages of this disease, the retinal microvasculature is affected by several abnormalities in the eye fundus such as the microaneurysms and/or dot hemorrhages, vascular hyper permeability signs, exudates, and capillary closures [1]. Microaneurysm dynamics primarily increase the risk that the laser photocoagulation requires progression to the level [2]. Diabetic retinopathy lesions are commonly accepted to be reversed and the progression of the retinopathy can only be slower during the early stages of the disease [3]. The identification by repeated examination of patients affected of these initial lesions (mainly Microaneurysms and small blood cells) is expected as a new possibility of improving retinopathy treatment. Floating and flashes, blurred vision, and loss of sudden vision can be common symptoms of diabetic retinopathy [4].

Early detection and treatment of DR are very important because it is a progressive disease and its severity depends on the number and types of lesions in the fundus image The main components of a healthy retina are blood vessels, optic discs, and macula, and any variations in these components are symptoms of eye disease. DR is divided widely into

The associate editor coordinating the review of this manuscript and approving it for publication was Wei Wei.

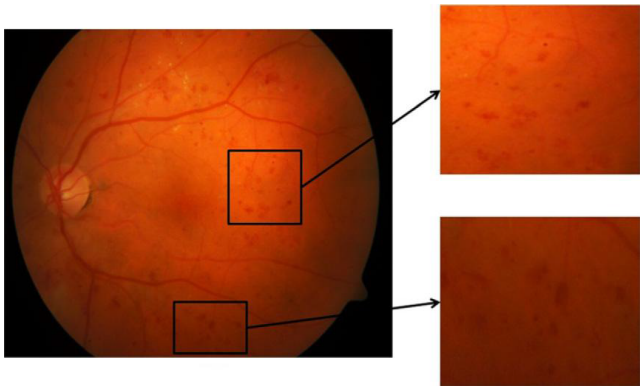

FIGURE 1. Enlarged regions of retinal image containing Mas [5].

two levels: DR (PDR) proliferative and DR (NPDR) non-proliferative. NPDR, referred to as the Diabetic Retinopathy background occurs when the blood vessels inside of the retina are weakened by diabetes, causing blood leakage and fluid on the retinal surface [6]. This leak reduces the sensitivity of the retina when wet and swollen. NPDR may include multiple retinopathic signs like hemorrhages(H), microaneurysms, cotton wool (CWS) or soft exudates, hard exudates (HE). Besides, NPDR is divided into three phases: mild, moderate and extreme, depending upon the occurrence and number of these lesions [7]–[10]. MAs are the first signs of NPDR and are caused by focal thin blood vessel dilation [11]–[14]. Tiny, nearly round-shaped and red-colored MAs. The following symbol is H, known as the dot or blot H. If the wall is excessively weakened with thin vessels or MAs, it can break and release H [8]. Dot bleeding looks like bright red spots and blot bleeding is bigger red hemorrhages. The hemorrhages and MA are sometimes considered to be one red lesion class recognized by HMA [15]–[19]. Figure 1 shows the Enlarged regions containing MAs.

In this paper, Microaneurysm quantification is not currently being applied in clinical practice, because of variability in detection and problems associated with angiography with fluorescein inter-and intra-observer [20]–[22]. Semantic segmentation of the medical image is the automated or semi-automatic method of identification of boundaries in 2D or 3D images. Image segmentation is a method for dividing a particular image into relevant regions with standardized features. A variety of attempts has been made to produce algorithms to automatically classify and track microaneurysms in the ocular fundus to resolve this variability. Deep Convolutional Neural Networks (DCNNs), a deep learning branch has impressive data on image analysis and interpretation applications, including medical imaging. Currently, large CNNs can successfully perform highly complex image recognition tasks with an outstanding norm for many object classes. In many typical image-classification projects, CNNs, like the annual ImageNet, are used [23], [24].

The major involvement of this paper is,

- To propose the Prognosis of Microaneurysm and early diagnosis system for non - proliferative diabetic retinopathy (PMNPDR) utilizing a deep convolutional neural network for semantic segmentation of fundus images which can increase the efficiency and accuracy of NPDR.
- Maximum matching filter response (MFR) mutual information (MI) and maximum Gaussian answer laplacian (LoG) in the 2-dimension function space utilizing Differential Evolution which, has not been previously explored in the detection of lesions.
- The experimental results have been performed based on the datasets (https://ieee-dataport.org) [25].

The rest of this paper decorated as follows: Section 1 and section 2 discussed the background and existing method of DR disease identification. In section 3 the Prognosis of Microaneurysm and early diagnosis system for non - proliferative diabetic retinopathy (PMNPDR) has been proposed. In Section 4 the experimental results has been demonstrated. Finally, section 5 completes the research paper.

II. LITERATURE REVIEW

Zhou *et al.* [26] proposed the sparse principal component analysis based unsupervised classification approach (SPCA-UCM) for microaneurysms (MA) detection. The characteristics of the sparse Principal Component Analysis which blends the elastic net penalty with Principle Component Analysis can be used to select effective features. Non-MAs data vary widely, the collection of non-microaneurysms training sets is quite subject to data, huge training sets not only take time and impact class imbalance problems. Since the non-MA class samples need not be taken into account, the class imbalance issue can be prevented.

Wilkinson *et al.* [27] introduced the Early Treatment Diabetic Retinopathy Study (ETDRS) based on the initial classification system. Build consensus regarding the classification of DR and diabetic macular edema clinical disease classification systems available around the world, and improve communication and coordination of treatment among doctors who care for diabetic patients. A research was carried out in advance of the Wisconsin Epidemiological Studies on Diabetic Retinopathy publications. Each Member reviewed it by e-mail. To stratify responses a changed Delphi framework was used. Separate diabetic retinopathy and macled edema systems were developed at a later workshop. The group members reassessed these and the modified Delphi system was used again to measure degrees of agreement.

Gulshan *et al.* [28] initialized the Deep Convolutional Neural Network (DCNN) for the recognition of DR in retinal fundus pictures. Deep learning can be used in retinal fundus photographs to create an algorithm to identify DR and diabetic macular edema automatically. Based on the major decision of the ophthalmologist team, the specificity and sensitivity of the algorithm for determining DR stated as moderate or worse DR or both were generated. The algorithm with 96.5% sensitivity and 92.4 % specificity is developed

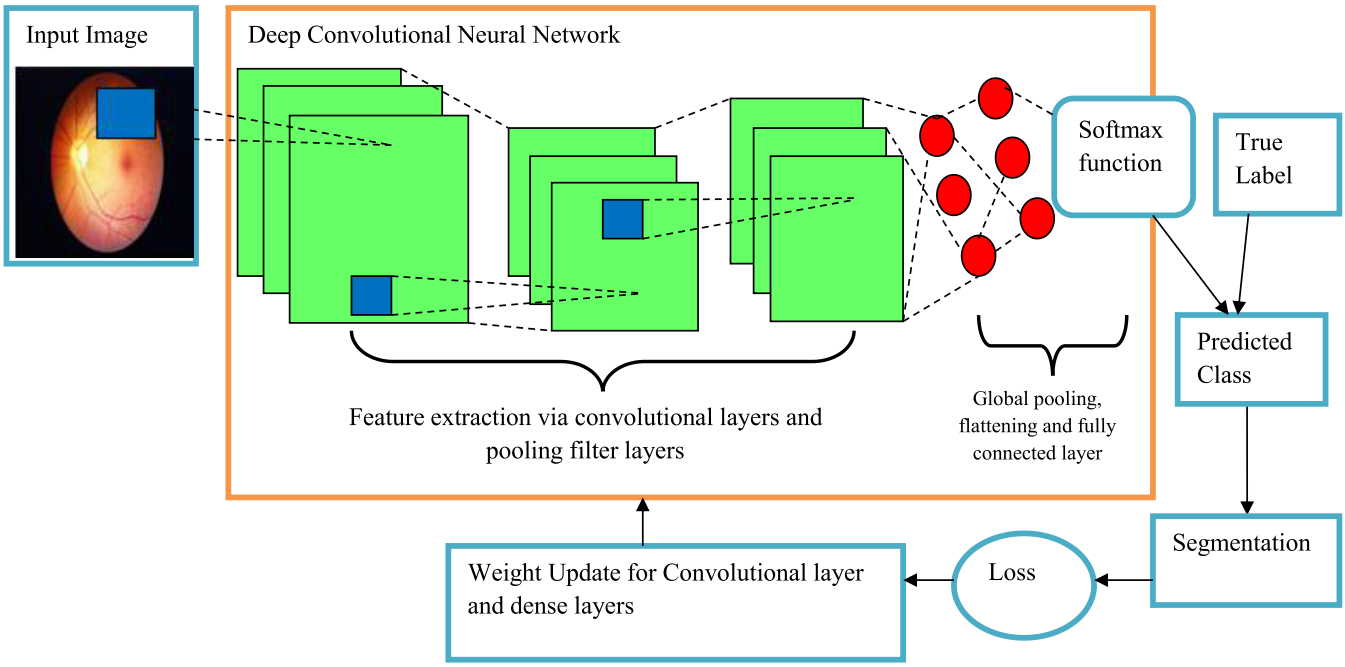

FIGURE 2. The classification methodology and deep convolutional neural network training process.

utilizing deep convolutional neural networks and a huge set of data in several grades per picture.

Agurto *et al.* [29] suggested the Multiscale Amplitude modulation-frequency -modulation (AM-FM) approach for discrimination between pathological and normal retinal pictures. The areas included microaneurysms, exudates, retinal neovascularization, hemorrhage, patterns of normal vessels and normal retinal background. The instantaneous amplitude cumulative distribution functions, the immediate frequency magnitude, and the relative instant frequency angles of several scales are utilized as texture feature vectors. They used inter structure similarity with distance metrics between extracted feature vectors. The results show that the pathological lesions and normal retinal structures are statistically different based on AM-FM characteristics.

Antal and Hajdu [30] introduced the ensemble-based system (EBS) for MA detection and DR grading. One way to guarantees high accuracy and reliability in a detector is to review ensemble-based systems in several fields that have proven to be effective. The traditional ensemble strategies, however, aim at combining real values or class labels, which can not be taken into account in our case. In MA identification, space coordinates are used as centers for potential MA candidates by detectors. A classification of each pixel would be appropriate for the application of well-known ensembles technology, which in our context can be confusing, since different algorithms may not fit different approaches with different MA-algorithms.

To overcome these issues, in this paper, Prognosis of Microaneurysm and early diagnosis system for non - proliferative diabetic retinopathy (PMNPDR) system that is capable to train effectively a deep convolution neural network for semantic segmentation of fundus images which can increase the efficiency and accuracy of NPDR (non proliferated diabetic retinopathy) detection. The identification of multiple retinal lesions in one frame continues to be an open question for DR research. In pathological retinal images, the texture of red lesions and bright blobs may be transient EXs or smooth can be modeled on the step edges in the retinal image while MAs display gaussian axial curves.

III. PROGNOSIS OF MICROANEURYSM AND EARLY DIAGNOSIS SYSTEM FOR NON - PROLIFERATIVE DIABETIC RETINOPATHY (PMNPDR)

In this paper, Prognosis of Microaneurysm and early diagnostics system for non-proliferative diabetic retinopathy (PMNPDR) capable of effectively creating a deep-convolutional neural network for the semantic segmentation of fundus images which can improve NPDR detection efficiency and accuracy. The input images entered will be fed into convolutional layers for analysis A unit of a convolutional layer in an input image binds to a small area called the receptive field, always extends to the entire image range. The units are placed in the feature maps in a convolutional layer The unit on the same map of features is on the same filter bank If flattened and analyzed with a fully connected layer that contains several class neurons, then the output of the last normally dual-module built to become a 336 dimensioned function vector in our job. Finally, the output of the fully associated layer is translated to the likelihood of every class by a Softmax function. The network will learn deeper features through increased convolutional layers. The convolution neurons are triggered by ReLU and the final layer connects to a softmax feature that transforms the performance in input image

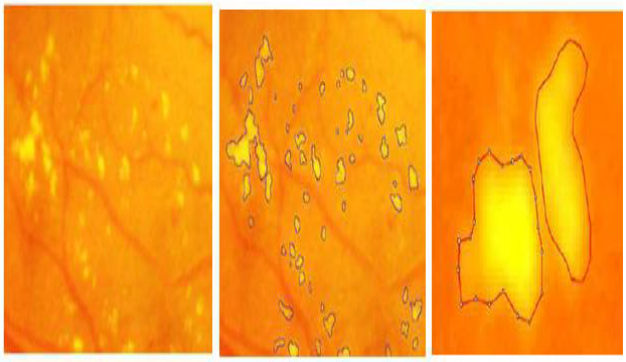

FIGURE 3. Detailed part of the fundus image of hard exudates: (a) hard exudate (EXs) presence; (b) hard exudate manual mark-ups; and (c) annotator view markup contour.

probabilities from different categories. The true label joins the expected Loss Calculation groups in training employing the objective function which in our case cross-entropy. The losses are then propagated back to the weights of the convolutional filter and fully connected layer by the network where stochastic gradient descent for weight updates has been used. The semantic segmentation of the diabetic retinopathy image has been performed. Figure 2 shows the classification methods and DCNNs training process. The dataset has been taken from https://ieee-dataport.org for the effective results [25].

A. PRE-PROCESSING

The exterior of various DR lesions varies, for example, because they are dark spots, and MA and hemorrhages are mostly undividable from the background while Exudates are a high-contrast yellow color. Therefore, some kind of edge improvement is required to distinguish between dark and background lesions. In contrast, pre-processing is not about edge processing, it rather about enhancing contrast. Figure 3 shows the detailed parts of the fundus image of hard exudates. Figure 3 (a) hard exudate (EXs) presence, figure 3 (b) is the hard exudate manual mark-ups and figure 3 (c) is the annotator view markup contour. Consequently, the following are done for various pre-processing operations:

1) ENHANCEMENT FOR DARK LESIONS ON THE EDGE OF CURVELET

The curve transform is efficient to define a horizontal, diagonal point and vertical, directional information, contours, missing, curvatures, and inaccurate boundary data, etc. The picture is first decomposed into several subbands with a curve transformation. The approximate subband is suppressed and some amplification factor increases the remaining (detailed) sub strip. This reinforces the borderline of the dark lesions that enhances their separation from the background.

2) OPTIMIZING BRIGHT LESIONS USING OPTIMAL BANDPASS FILTER

Morphological closures are carried out on the image under consideration to preserve the luminous regions. It smoothes the substrate suppresses and components the thin (lack-out) vascular networks so that light lesions remain virtually unchanged. This closing process, however, it reduces the picture contrast. The image is transferred via an optimal wideband bandpass filter structure to enhance the contrast of the Exudates. Exudates often cover a wide range of retinal picture frequency spectrums. The optimal gain (H), the lower and the high cut-out frequencies f_L and f_u are difficult and computationally complex to analytically measure because several parameters are used, the band-pass filters (BPF) for individual images.

This work defines gains and cutoff frequencies for each image by optimizing the mean structural similarity measurement (MSSIM) as well as the two cutoff frequencies of optimum BPF for individual images. It is divided into l blocks of size $m \times m$ and the following is determined by Structural Similarity Measurement (SSIM).

$$SSIM = \frac{(2\bar{y}\bar{x} + B_1)(2\rho_{yx} + B_2)}{\left(\rho_y^2 + \rho_x^2 + B_2\right)((\bar{y})^2 + (\bar{x})^2 + B_1)} \quad (1)$$

As shown in equation (1) where ρ_x and ρ_y denote standard deviations in the original and enhanced blocks correspondingly.ρ_{yx} respective to the covariance estimation of pixel intensities and $\bar{y}$ and $\bar{x}$ are the mean values. The variable B_1 and B_2 are involving to prevent instabilities when $((\bar{y})^2 + (\bar{x})^2$ and $\rho_y^2 + \rho_x^2$ belongs to zero.

B. CANDIDATE LESIONS DETECTION

The following steps are taken in the detection of candidate lesions:

1) GAUSSIAN FILTERING MATCHED FILTERS AND LAPLACIANS

A matched Filter with a 2-dimensional Gaussian kernel has high responsiveness to dark as well as bright lesions that can be formed respectively as step borders and Gaussian. This way, LoG filters together with Matched Filter are utilized to identify the transient bright lesions and the Gaussian intensity-like dark lesions. The 2-dimensional MF and LoG prototype kernel mathematical expressions are given respectively via equation (2) and (3).

$$L(y, x) = -\exp\left(-\frac{y^2}{2\rho}\right), for\ |y| \le (3\rho) \quad (2)$$

$$T(y, x) = \frac{1}{\rho\sqrt{2\pi}}\left(\frac{y^2 - \rho^2}{\rho^4}\right)\exp\left(\frac{y^2}{2\rho^2}\right) \forall\ |y| \le 3\rho \quad (3)$$

Matched filters and LoG filters with a single Gaussian Kernel ρ (=1.5) are appropriate for Ex and HEM detection. Gaussian multiple value ρ kernels are required for sufficient MA detection, however, as MAs differ largely in shape and sizes.

2) MAXIMIZING MUTUAL INFORMATION

Mutual Information denoted by J(Y; X) for the discrete independent random variables (Y; X) with likelihood distribution

q(y) and q(x) correspondingly is stated as

$$J\,(Y;X) = G\,(Y) + G\,(X) - G(Y,X) \tag{4}$$

As shown in equation (4) where G(Y) and G(X) are the entropy of Y and X correspondingly. G(Y; X) is the joint entropy.

Let's consider the classifying every Y and X into two classes, called background (AL) and EX. The objective is to determine the optimum threshold R_1 and R_2 that partition Y and X into AL and EXs like J(Y; X) is increased J(Y; X) can be depicted as,

$$J\,(Y;X) = J(Y;X)_{AL} + J(Y;X)_{EX} \tag{5}$$

Differential Evolution is checked for the maximal values of these parameters. From the following equation can be determined the R_m the threshold that divides each of the functional spaces into AL and EX.

$$R_m = \frac{b_m - c_m}{2} \tag{6}$$

The value m = 1 for Y and m = 2 for X are utilized. The equation (5) can be rewritten as,

$$J(Y;X)_{AL} = G(Y)_{AL} + G(X)_{AL} - G(Y,X)_{AL} \tag{7}$$

where

$$G(Y)_{AL} = -\sum_{y=n_1}^{a_1} q(y)\log q(y) \tag{8}$$

$$G\,(X)_{AL} = -\sum_{x=n_2}^{a_2} q\,(y,x)\log q(x) \tag{9}$$

$$\begin{aligned} G(Y,X)_{AL} &= -\sum_{x=n_2}^{a_2}\sum_{y=n_1}^{a_1} q\,(y,x)\log q(y,x) \\ &= -\sum_{x=n_2}^{a_2}\sum_{y=n_1}^{a_1} q\,(y)\,q\,(x)\log\left[q\,(y)\,q\,(x)\right] \\ &= -\sum_{x=n_2}^{a_2}\sum_{y=n_1}^{a_1} q\,(y)\,q\,(x) \\ &\quad\times\left[\log q\,(y) + \log q\,(x)\right] \\ &= -\sum_{x=-n_2}^{a_2}\sum_{y=n_1}^{a_1} q\,(y)\,q\,(x)\,logq(y) \\ &\quad -\sum_{x=n_2}^{a_2}\sum_{y=n_1}^{a_1} q\,(y)\,q\,(x)\log q(x) \\ &= -\sum_{x=n_2}^{a_2} q(x)\sum_{y=n_1}^{a_1} q\,(y)\log q(y) \\ &\quad -\sum_{x=n_2}^{a_2} q\,(x)\log q(x)\sum_{y=n_1}^{a_1} q(y) \\ &\quad -\sum_{x=n_2}^{a_2} q(x)\sum_{y=n_1}^{a_1} q(y)\log q\,(y) \\ &\quad -\sum_{x=n_2}^{a_2} q\,(x)\log q(x)\sum_{y=n_1}^{a_1} q(y) \end{aligned} \tag{10}$$

The expression can be obtained in terms of $J(Y;X)_{EX}$.

As shown in the above equation Optimization of DE: The optimal values for b_m and a_m, which give the optimal R_m value, are defined for the partition of both AL and EX classes with a minimum overlapping area.

As shown in algorithm 1 where the optimal values of $b_m$and a_m, are determined by Differential Evolution similar to how the optimal Band Pass Filter is designed for the improvement of bright lesions. Here, the four parameters are b_1, a_1, b_2, and a_2 for each chromosome. The goal is to maximize the J(Y; X)

Algorithm 1 Lesions Detection Algorithm

Input:a,b,x,y
Output:G, J(Y;X)
For (a = 0)
$L\,(y,x) = -\exp\left(-\frac{y^2}{2\rho}\right)$
For (b = 0)
$T\,(y,x) = \frac{1}{\rho\sqrt{2\pi}}\left(\frac{y^2-\rho^2}{\rho^4}\right)\exp\left(\frac{y^2}{2\rho^2}\right)$
for (T=1) $J(Y;X)_{AL} = G(Y)_{AL} + G(X)_{AL} - G(Y,X)_{AL}$
If (t = 0)

$$\begin{aligned} G(Y,X)_{AL} = &-\sum_{x=n_2}^{a_2} q(x)\sum_{y=n_1}^{a_1} q(y)\log q\,(y) \\ &-\sum_{x=n_2}^{a_2} q\,(x)\log q(x)\sum_{y=n_1}^{a_1} q(y) \end{aligned}$$

Else $t \neq 0$
End for
End for
End if
End for
End
Return

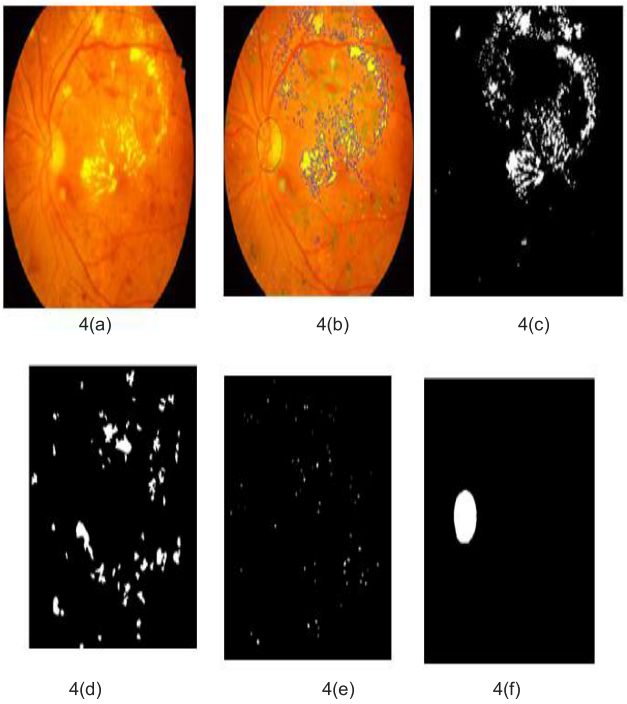

FIGURE 4. Photograph of retinal and various annotations (a) sample fundus image from the data sets presented; (b) annotator ground markups; (c – f) hard exudate ground tests, hemorrhage, soft exudates and microaneurysms, respectively optical discs.

value and to represent the fitness value of each chromosome. In each iteration, b_m and a_m values are updated by mutation and intersection. For the next iteration, the chromosomes showing better fitness between the two iterations are chosen.

The lesion detection system, consisting of four main stages: optical disc removal and vessel extraction, candidate

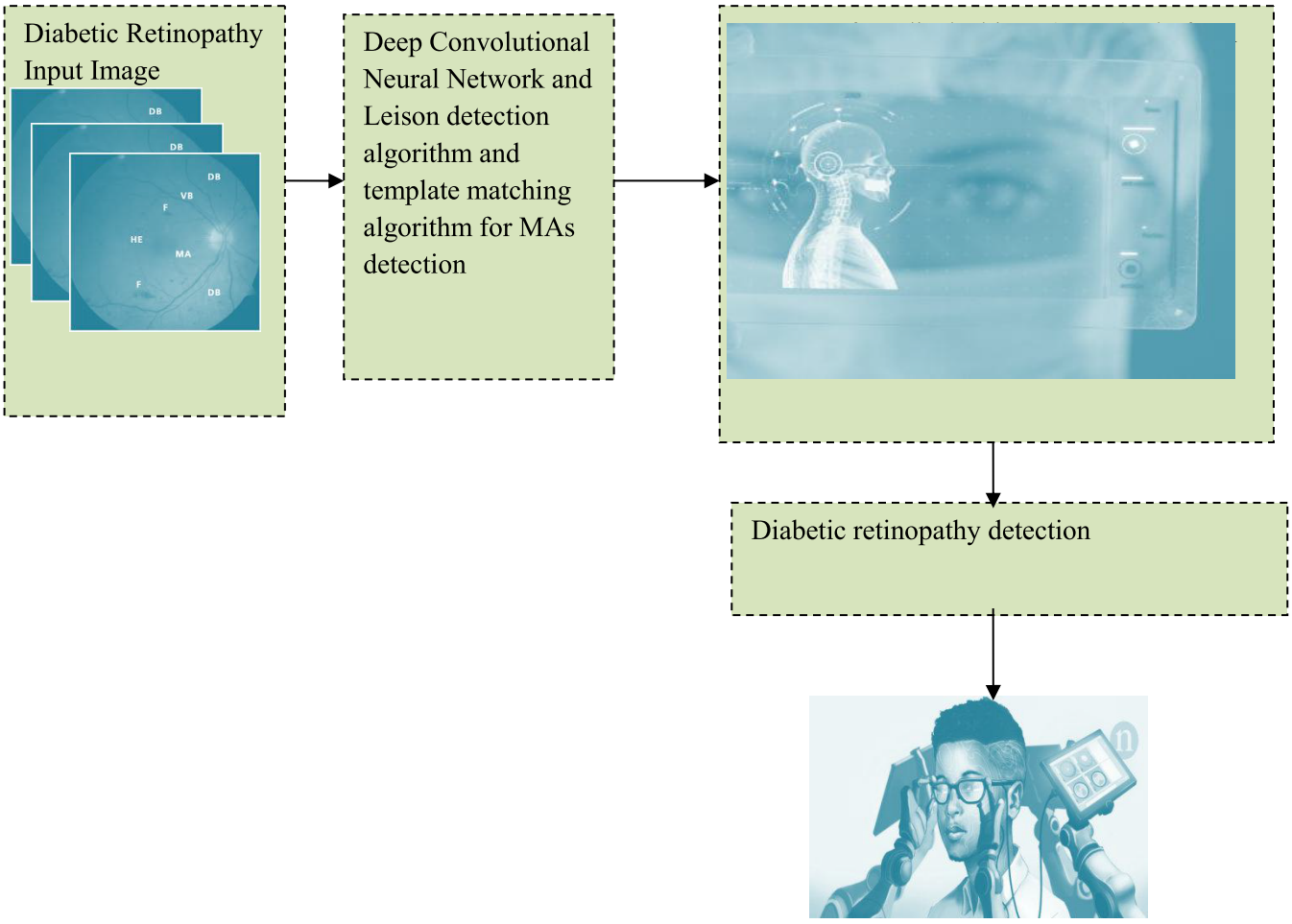

FIGURE 5. The proposed system for prediction of DR.

lesion detection, pre-processing, and post-processing, play a major role in early DR detection. The blood vessels and optical discs are initially blocked for further examination. The DR signs include red lesions like MA and blood flows, bright lesions such as cotton wool spots and hard exudates in color fundus pictures. Between lesions are MA that appears on the retinal surface as small circular dark spots. Figure 4 shows the retinal image with various annotations. Figure 4 (a) is the sample fundus image from the data sets presented and Figure 4 (b) is the annotator ground markups. Figure 4 (c to f) is the hard exudate ground tests, hemorrhage, soft exudates and microaneurysms, respectively optical discs.

C. CANDIDATE EXTRACTION

The first step is to measure the correlation coefficient of each pixel by using a non-linear filter with various Gaussian kernels. The cumulative coefficient between the five responses is chosen to provide the end response at each pixel position. As MAs are of different sizes, the end response with various Gaussian kernels provides Microaneurysms of different sizes to be detected. Here it refers to the function of Gaussians and the gray distribution of the MAs by the A and B variables. The coefficient of correlation can be stated as:

$$coeff_{BA} = \frac{\sum_n \sum_m \left(B_{nm} - \bar{B}\right)\left(A_{nm} - \bar{A}\right)}{\sqrt{\left(\sum_n \sum_m \left(B_{nm} - \bar{B}\right)^2\right)\left(\sum_n \sum_m \left(A_{nm} - \bar{A}\right)^2\right)}} \tag{11}$$

Additionally, to decrease the number of final response candidates for microaneurysm. To exclude candidates with low coefficients, an R limit ranging from 0.1 to 0.9 with an interval of 0.1 is applied. As the MAs are not included in the vasculature, all candidates must be excluded. However, the size and type of the microaneurysm candidates detected are not the true MA. The increasing area is therefore used to solve this problem. In the can area, the image J_{bg} context can be acquired with the use of a medium filter to an image J_{green}. Equation (2) offers a dynamic-based adaptive threshold r. The following equation expressed as:

$$r = J_{darkest} - \alpha \cdot \left(J_{darkest} - j_{bg}\right) \tag{12}$$

As shown in equation (12) where α is a constant value differing from 0 to 1. $J_{darkest}$ indicates the low intensity for every candidate region in J_{green}. J_{bg} is background intensity.

1) PRINCIPLE COMPONENT ANALYSIS

Principle Component Analysis is a method of linear reduction of dimensionality. The basic principle is that the forecasts on new directions differ as much as possible. Given many $Y \in T^{M\times n}$ samples with M samples and n variables, the target optimization function can be set as the following expression.

$$max_{u\neq 0}\frac{u^R Y^R Y_u}{u^R u} \tag{13}$$

Singular Value Decomposition (SVD) will measure equation (3) constant solution.

$$\frac{1}{\sqrt{m-1}}Y = V\Sigma U^R \tag{14}$$

As shown in equation (14) where $V \in T^{m\times m}$ and $U \in T^{n\times n}$ are all unitary matrix.

Select a new $Q \in T^{n\times b}$ for the new load matrix called the principal component subspace (PCS), which will be the first of U columns.

$$R = YQ \tag{15}$$

The PCS can be projected with a new sample vector y:

$$r = Q^R y \in PCS \tag{16}$$

For value b the following is determined by the Cumulative Percent Variance (CPV):

$$CPV\ (b) = 100\left[\frac{\sum_{i=1}^{b}\lambda_i}{\sum_{i=1}^{n}\lambda_i}\right]\% \tag{17}$$

2) SPARSE PCA

There are many features that are linearly relevant with relatively large noises. These variables are considered to be weakly relevant Because PCA primarily aims at achieving the maximum variance for certain loading vectors, certain key components will inevitably come with such poor relevant variables to minimize detection accuracy. The objective function expressed as equation (18)

$$\sum_{i=1}^{n}|u_i| \leq sparsity \tag{18}$$

Note that every Principle Component is a linear combination of n variables, so the PC can be regressed to n values for sparse loading. Enable $Z_j = YU_j =$ to indicate the principal component of the jth to be a positive constant for each j. The ridge determination $\hat{\mu}_{ridge}$ are provided by the following:

$$\hat{\mu}_{ridge} = \arg\max_{\mu}\left\|Z_j - Y_\mu\right\|^2 + \lambda\left\|\mu\right\|^2 \tag{19}$$

As shown in equation (19) where $\hat{\mu}_{ridge}$ can be estimated by $\hat{u} = \frac{\hat{\mu}_{ridge}}{\left\|\hat{\mu}_{ridge}\right\|^2}$, $\hat{u} = U_j$is the jth loading.

When a linear regression model contains multiple correlated variables, the coefficients can be poorly defined and have large variations. An equally large negative factor on its associated cousin may nullify a relatively large positive coefficient of one variable. The following equation obtains the objective function,

$$\hat{\mu} = \arg\max_{\mu}\left\|R_j - Y_\mu\right\|^2 + \lambda\left\|\mu\right\|^2 + \tau\left\|\mu\right\| \tag{20}$$

Algorithm 2 Template Matching Algorithm for MA Detection

Input:j, μ, λ
Output: r, Y
For (j = 1)
$r = J_{darkest} - \alpha\cdot\left(J_{darkest} - j_{bg}\right)$
For (j = 0)
$max_{u\neq 0}\frac{u^R Y^R Y_u}{u^R u}$
For ($\lambda = 0$)
$R = YQ$
If (r = 0)
$\hat{\mu}_{ridge}\arg\max_{\mu}\left\|Z_j - Y_\mu\right\|^2 + \lambda\left\|\mu\right\|^2$
Else ($\mu = 0$)
$\hat{\mu} = \arg\max_{\mu}\left\|R_j - Y_\mu\right\|^2 + \lambda\left\|\mu\right\|^2 + \tau\left\|\mu\right\|$
End for
End if
End for
End for
End
Return

As shown in the algorithm 2, the wavelet detection of MAs, local template matching has been used. This method will effectively avoid the issue of illumination variations or high-frequency noise. The Gaussian Correlation Coefficients Multi-scale method (MSCF) was used for the identification of MAs. In this study, MA applicants can be identified by using five various Gaussian kernels for every pixel to determine the maximum correlation coefficient. It is not appropriate to simplify the consideration of all features. There are invariably obsolete or redundant features to be added that not only deteriorate classification efficiency and take time. So it is important to consider how to select the appropriate subcomponent of functions for the candidate class.

As shown in figure 5 the proposed scheme provides an effective system for early prediction of diabetic retinopathy. Combining a high-quality retinal with a readable artificial intelligence app, the smartphone installed system can in real-time assess whether a patient should be referred for follow-up to an ophthalmologist. A proprietary deep neural network technology called EyeArt is used for the RetinaScope app. After pupil dilation, the spectrum of the patient retinal images was used and images has been analyzed with software that categorized them as RWDR or DR with non-referral warranties.

IV. EXPERIMENTAL RESULTS AND DISCUSSION

Figure 6 shows the semantic segmentation process of diabetic retinopathy detection and the final result. The original image

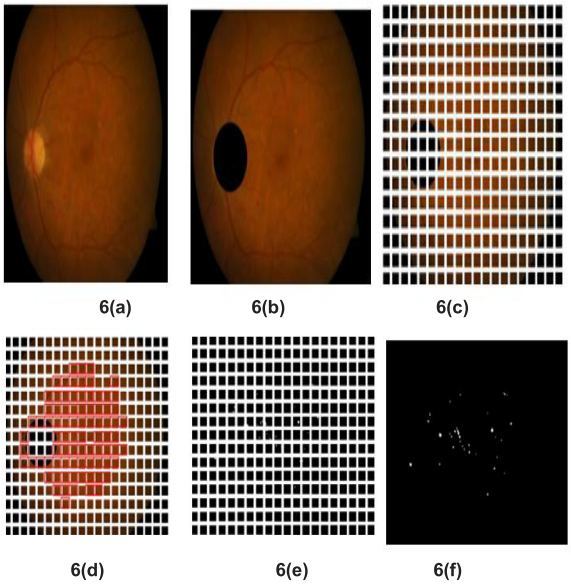

FIGURE 6. Result of proposed method: (a) Original images (b) removal of the optic disc (c) divided images (d) classification results of the exudates patch (e) Semantic segmentation utilizing template matching algorithm of every patch (f) final segmentation image.

6(a) which is obtained from the datasets [25] and 6(b) is the removal of the optic disc. The resulting image is separated into smaller parts, called patch as shown in Figure 6(c), once the optical disk has been removed from the original image. 32×32 pixel patch size is set exudates patch classification as shown in figure 6(d). Subsequently, a strength level is defined to acquire exudates, which are used in the semantic segmentation process is shown in figure 6(e). The patch is separated by the map of the template matching algorithm and then all patches are merged into one whole frame, as shown in Figure 6(f).

A. RELATIVE SPECIFICITY AND SENSITIVITY RATIO

$$Sensitivity = \frac{True\ positive}{True\ positive + False\ negative} \tag{21}$$

$$Specificity = \frac{True\ negative}{True\ negative + False\ positive} \tag{22}$$

Note that, depending on the task, detecting the DR is either a fundus picture, a patch, or a picture pixel. Sensitivity(SN) tests the fraction of the correct classification of positive instances, or the true positive rate or the recall; Specificity(SP) or precision or the positive predictive value estimates the fraction of properly classified positive value or the true negative rate estimates the fraction of properly classified negative value. On average sensitivity values of 97.4%, 98.4% and 95.1%, respectively for detecting dark lesions and 96.8%, 97.1% and 95.3% for detecting bright lesions, respectively are of specificity and precision for the proposed method. Figure 7 (a) demonstrates the relative sensitivity ratio and Figure 7(b) demonstrates the relative specificity ratio.

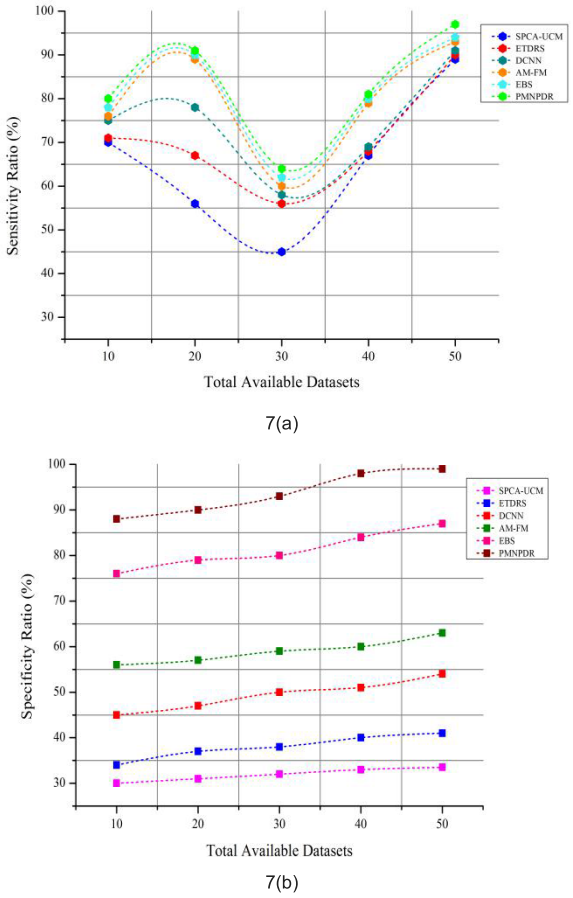

FIGURE 7. (a) Relative sensitivity ratio (b) Relative specificity ratio.

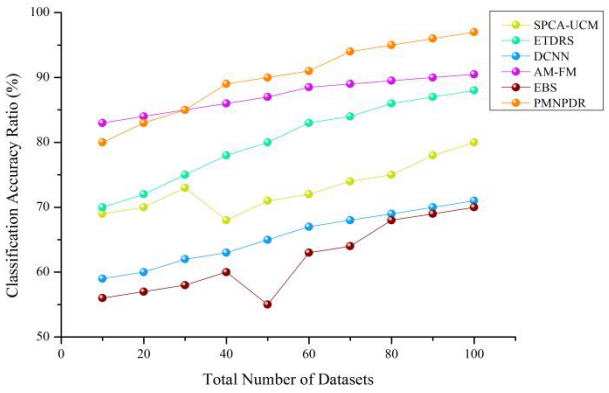

FIGURE 8. Classification accuracy ratio.

B. CLASSIFICATION ACCURACY RATIO

Accuracy of both automatic and manual segments depends on spatial resolution and image contrast. The segmentations obtained from various resolutions/contrasts are therefore not directly comparable. A quantitative evaluation has been presented and comparison with competitors like GMM and a classifier, SVM, of the proposed multivariate classification algorithms based on m-mediums.

The proposed approach to the combination of the classification systems to improve classification accuracy in MA

TABLE 1. Accuracy evaluation.

Total Number of Dataset	SPCA-UCM	ETDRS	DCNN	AM-FM	EBS	PMNPDR
10	69.2	70.1	59.3	83.4	56.4	80.3
20	70.1	72.3	60.2	84.5	57.9	83.3
30	73.3	75.9	63.6	85.3	58.2	85.6
40	68.9	78.2	65.9	86.2	60.2	89.7
50	71.2	80.3	68.7	87.1	55.2	90.2
60	74.8	83.4	69.2	88.9	56.9	92.3
70	74.3	85.4	70.1	88.2	63.7	94.1
80	75.8	86.2	72.1	89.1	65.8	95.9
90	78.9	87.1	73.2	89.9	67.9	96.5
100	80.5	88,2	74.9	90	70.1	97.8

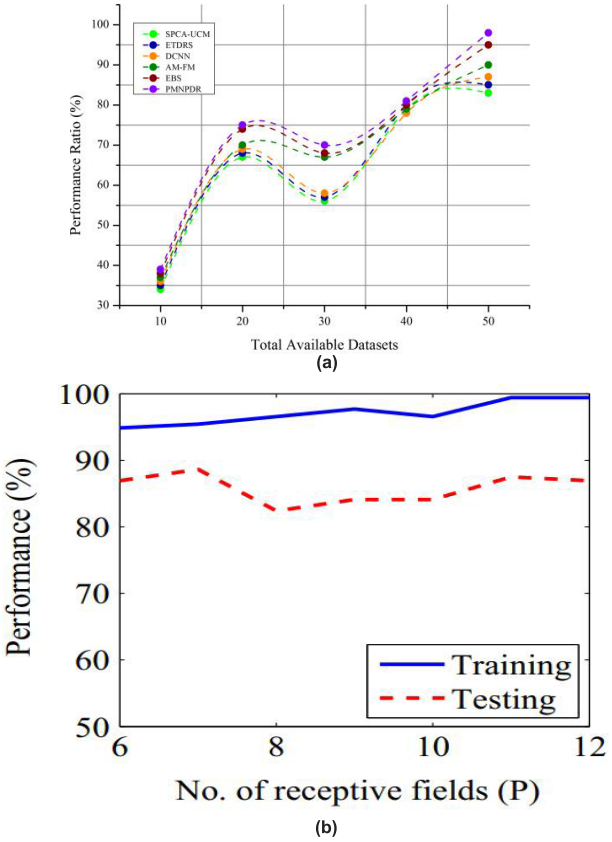

FIGURE 9. (a) Performance Ratio (b) overall training and testing accuracy.

TABLE 2. Performance analysis.

Total Number od Dataset	SPCA-UCM	ETDRS	DCNN	AM-FM	EBS	PMNPDR
10	34.6	35.3	36.7	37.2	38.9	40.2
20	67.3	68.2	69.8	70.8	74.5	75.6
30	56.7	57.1	58.3	67.3	68.7	70.1
40	79.8	80.9	78.2	79.3	80.9	81.2
50	83.4	85.3	87.6	90.1	95.6	98.7

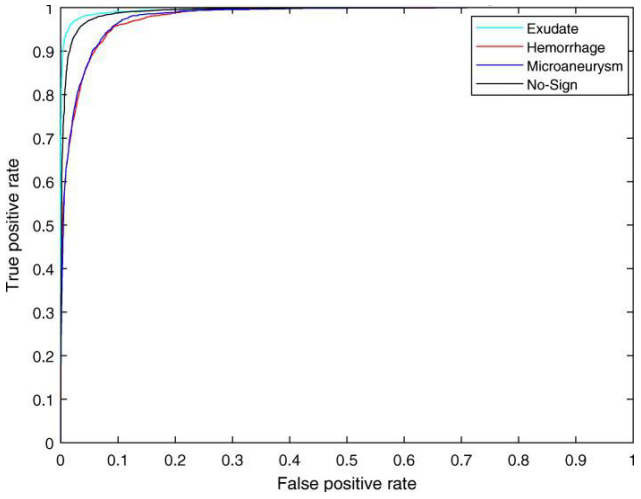

FIGURE 10. ROC curve.

regions demonstrates its effectiveness. Figure 8 shows the accuracy ratio of the proposed PMNPDR system.

Table 1 demonstrates the classification accuracy evaluation of the proposed PMNPDR system. The purpose was to estimate how well MAs has been identified in the sequential images using a picture analysis algorithm and therefore their ability to evaluate rotation. Applied to all the image pairs of the test sample, an algorithm summarizing the number of new, static and resolved MAs per pair was presented.

C. PERFORMANCE RATIO

A comparison of performance for the detection of dark lesions indicates that the proposed solution exceeds existing technology. In terms of specificity and sensitivity measurements for bright lesion identification, the efficiency of the proposed PMNPDR approach is competitive and demonstrates enhanced performance has been compared to other existing methods. The proposed system's statistical performance is analyzed with Receivers Operating Characteristics

(ROCs), which is the graph of True Positive Rate against False Positive Rate. Depending on the assessment of the lesion level, the ROC curves are shown in Figure 9 (a). Figure 9(b) shows the overall testing and training accuracy of the proposed PMNPDR approach.

Table 2 shows the performance ratio of the proposed PMNPDF system. The classification model proposed demonstrates its efficiency in MAs turnover recognition. Since the classification model is free to purchase and maintain the program for image processing, and automated test method on the development of diabetic retinopathy would be promising given that MAs are the early biomarker of diabetic retinopathy.

D. RECEIVER OPERATING CHARACTERISTIC

Through evaluating the receiver operating characteristics (ROC), a plot of false-positive rates against true positive values, the output of classifiers on the same data can be established. When the curve is close, the more precise the test is, the y-axis follows the top border of the ROC. The closer the curve comes to the diagonal of 45 degrees of the ROC space, the more precise the test. There is a measure of accuracy in the AUC. Figure 10 demonstrates the performance of the proposed algorithms through the ROC curve.

V. CONCLUSION

This paper presents the Prognosis of Microaneurysm and early diagnostics system for non-proliferative diabetic retinopathy (PMNPDR) capable of effectively creating DCNNs for the semantic segmentation of fundus images which can improve NPDR detection efficiency and accuracy. An easy yet efficient integrated lesion identification system, coupled with LOG and MF filters accompanied by post-processing procedures, is suggested. Combined sequentially and smartly, these techniques provide a very effective system for the identification of various lesions regardless of their texture, form, scale, etc. Transforming Curvelets is a very good candidate for better dark lesions. The BPF is optimally designed for the improvement of bright lesions. Through MSSIM maximization, the BPF's gain and cutting frequencies are automatically achieved. Data for non-MAs vary widely, the collection of non-microaneurysm training is quite a topic. The huge training set not only takes time and causes class imbalance. In this paper, a sparse Principal Component Analysis based unregulated classification approach for detecting microaneurysm was developed. Once a model that represents MA has been developed, any deviating from the standard MA is detected by statistical monitoring, a scarce Principal Component Analysis is employed to find the latent structure of microaneurysm data.

ACKNOWLEDMENT

(Lifeng Qiao and Ying Zhu contributed equally to this work.)

REFERENCES

[1] G. García, J. Gallardo, A. Mauricio, J. López, and C. Del Carpio, "Detection of diabetic retinopathy based on a convolutional neural network using retinal fundus images," in *Proc. Int. Conf. Artif. Neural Netw.* Cham, Switzerland: Springer, Sep. 2017, pp. 635–642.

[2] S. S. Kar and S. P. Maity, "Automatic detection of retinal lesions for screening of diabetic retinopathy," *IEEE Trans. Biomed. Eng.*, vol. 65, no. 3, pp. 608–618, Mar. 2018.

[3] C. I. Serrano, V. Shah, and M. D. Abràmoff, "Use of expectation disconfirmation theory to test patient satisfaction with asynchronous telemedicine for diabetic retinopathy detection," *Int. J. Telemed. Appl.*, vol. 2018, pp. 1–14, Oct. 2018.

[4] M. Islam, A. V. Dinh, and K. A. Wahid, "Automated diabetic retinopathy detection using bag of words approach," *J. Biomed. Sci. Eng.*, vol. 10, no. 05, pp. 86–96, 2017.

[5] M. U. Akram, S. Khalid, and S. A. Khan, "Identification and classification of microaneurysms for early detection of diabetic retinopathy," *Pattern Recognit.*, vol. 46, no. 1, pp. 107–116, Jan. 2013.

[6] S. D. Solkar and L. Das, "Survey on retinal blood vessels segmentation techniques for detection of diabetic retinopathy," *Diabetes Int. J. Electron. Electr. Comput. Syst.*, vol. 6, no. 6, pp. 490–495, 2017.

[7] P. Costa, A. Galdran, A. Smailagic, and A. Campilho, "A weakly-supervised framework for interpretable diabetic retinopathy detection on retinal images," *IEEE Access*, vol. 6, pp. 18747–18758, 2018.

[8] M. C. Savastano, M. Federici, B. Falsini, A. Caporossi, and A. M. Minnella, "Detecting papillary neovascularization in proliferative diabetic retinopathy using optical coherence tomography angiography," *Acta Ophthalmologica*, vol. 96, no. 3, pp. 321–323, May 2018.

[9] C. Burnscox, S. Safi, A. Hafezi-Moghadam, and H. Ahmadieh, "Early detection of diabetic retinopathy," *Lancet*, vol. 324, no. 8404, pp. 693–694, Sep. 1984.

[10] J. Amin, M. Sharif, M. Yasmin, H. Ali, and S. L. Fernandes, "A method for the detection and classification of diabetic retinopathy using structural predictors of bright lesions," *J. Comput. Sci.*, vol. 19, pp. 153–164, Mar. 2017.

[11] P. Costa and A. Campilho "Convolutional bag of words for diabetic retinopathy detection from eye fundus images," *IPSJ Trans. Comput. Vis. Appl.*, vol. 9, no. 1, pp. 1–6, 2017.

[12] D. S. W. Ting *et al.*, "Development and validation of a deep learning system for diabetic retinopathy and related eye diseases using retinal images from multiethnic populations with diabetes," *J. Amer. Med. Assoc.*, vol. 318, no. 22, pp. 2211–2223, Dec. 2017.

[13] P. Costa, T. Araujo, G. Aresta, A. Galdran, A. M. Mendonca, A. Smailagic, and A. Campilho, "EyeWeS: Weakly supervised pre-trained convolutional neural networks for diabetic retinopathy detection," in *Proc. 16th Int. Conf. Mach. Vis. Appl. (MVA)*, May 2019, pp. 1–6.

[14] F. D. Verbraak, M. D. Abràmoff, G. C. F. Bausch, C. Klaver, G. Nijpels, R. O. Schlingemann, and A. A. van der Heijden, "Diagnostic accuracy of a device for the automated detection of diabetic retinopathy in a primary care setting," *Diabetes Care*, vol. 42, no. 4, pp. 651–656, Apr. 2019.

[15] S. Wan, Y. Liang, and Y. Zhang, "Deep convolutional neural networks for diabetic retinopathy detection by image classification," *Comput. Electr. Eng.*, vol. 72, pp. 274–282, Nov. 2018.

[16] M. D. Abràmoff, P. T. Lavin, M. Birch, N. Shah, and J. C. Folk, "Pivotal trial of an autonomous AI-based diagnostic system for detection of diabetic retinopathy in primary care offices," *NPJ Digit. Med.*, vol. 1, no. 1, p. 39, 2018.

[17] A. Rakhlin, "Diabetic retinopathy detection through integration of deep learning classification framework," *bioRxiv*, Jun. 2018, Art. no. 225508.

[18] D. Doshi, A. Shenoy, D. Sidhpura, and P. Gharpure, "Diabetic retinopathy detection using deep convolutional neural networks," in *Proc. Int. Conf. Comput., Anal. Secur. Trends (CAST)*, Dec. 2016, pp. 261–266.

[19] R. Pires, S. Avila, J. Wainer, E. Valle, M. D. Abràmoff, and A. Rocha, "A data-driven approach to referable diabetic retinopathy detection," *Artif. Intell. Med.*, vol. 96, pp. 93–106, May 2019.

[20] G. Quellec, K. Charrière, Y. Boudi, B. Cochener, and M. Lamard, "Deep image mining for diabetic retinopathy screening," *Med. Image Anal.*, vol. 39, pp. 178–193, Jul. 2017.

[21] C. Bedard, S. S. Liu, C. Patterson, H. Gerstein, and L. Griffith, "Systematic review: Can non-mydriatic cameras accurately detect diabetic retinopathy?" *Diabetes Res. Clin. Pract.*, vol. 129, pp. 154–159, Jul. 2017.

[22] H. S. Sandhu, N. Eladawi, M. Elmogy, R. Keynton, O. Helmy, S. Schaal, and A. El-Baz, "Automated diabetic retinopathy detection using optical coherence tomography angiography: A pilot study," *Brit. J. Ophthalmol.*, vol. 102, no. 11, pp. 1564–1569, Nov. 2018.

[23] M. D. Abràmoff, Y. Lou, A. Erginay, W. Clarida, R. Amelon, J. C. Folk, and M. Niemeijer, "Improved automated detection of diabetic retinopathy on a publicly available dataset through integration of deep learning," *Investigative Opthalmol. Vis. Sci.*, vol. 57, no. 13, pp. 5200–5206, Oct. 2016.

[24] Z. Wang, Y. Yin, J. Shi, W. Fang, H. Li, and X. Wang, "Zoom-in-net: Deep mining lesions for diabetic retinopathy detection," in *Proc. Int. Conf. Med. Image Comput. Comput.-Assist. Intervent.* Cham, Switzerland: Springer, Sep. 2017, pp. 267–275.
[25] *Indian Diabetic Retinopathy Image Dataset Idrid*. Accessed: Nov. 2019. [Online]. Available: https://ieee-dataport.org/open-access/indian-diabetic-retinopathy-image-dataset-idrid
[26] W. Zhou, C. Wu, D. Chen, Y. Yi, and W. Du, "Automatic microaneurysm detection using the sparse principal component analysis-based unsupervised classification method," *IEEE Access*, vol. 5, pp. 2563–2572, 2017.
[27] C. P. Wilkinson, F. L. Ferris, R. E. Klein, P. P. Lee, C. D. Agardh, M. Davis, D. Dills, A. Kampik, R. Pararajasegaram, and J. T. Verdaguer, "Proposed international clinical diabetic retinopathy and diabetic macular edema disease severity scales," *Ophthalmology*, vol. 110, no. 9, pp. 1677–1682, Sep. 2003.
[28] V. Gulshan, L. Peng, M. Coram, M. C. Stumpe, D. Wu, A. Narayanaswamy, S. Venugopalan, K. Widner, T. Madams, J. Cuadros, R. Kim, R. Raman, P. C. Nelson, J. L. Mega, and D. R. Webster, "Development and validation of a deep learning algorithm for detection of diabetic retinopathy in retinal fundus photographs," *J. Amer. Med. Assoc.*, vol. 316, no. 22, pp. 2402–2410, 2016.
[29] C. Agurto, V. Murray, E. Barriga, S. Murillo, M. Pattichis, H. Davis, S. Russell, M. D. Abràmoff, and P. Soliz, "Multiscale AM-FM methods for diabetic retinopathy lesion detection," *IEEE Trans. Med. Imag.*, vol. 29, no. 2, pp. 502–512, Feb. 2010.
[30] B. Antal and A. Hajdu, "An ensemble-based system for microaneurysm detection and diabetic retinopathy grading," *IEEE Trans. Biomed. Eng.*, vol. 59, no. 6, pp. 1720–1726, Jun. 2012.

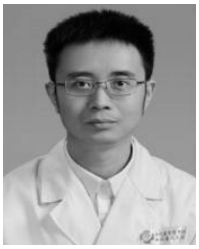

LIFENG QIAO received the master's degree in ophthalmology from the Zunyi Medical College, in July 2007. He has been working at the Department of Ophthalmology, Sichuan Provincial People's Hospital, since September 2007. His research direction is ocular fundus medical diseases and surgical treatment of vitreoretinal diseases. In 2019, he served as the Secretary of the Ophthalmology Branch of the Sichuan Medical Association and a member of the Youth Committee of the Ophthalmology of the Sichuan Medical Association.

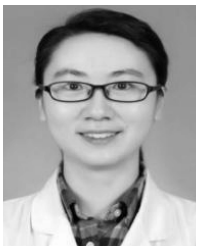

YING ZHU received the M.D. degree from the Tongji Medical College, Huazhong University of Science and Technology, in June 2012. Since July 2012, she has been with the Department of Endocrinology, Sichuan Academy of Medical Sciences and Sichuan Provincial People's Hospital. In 2018, she has served as a Young Editorial Board Member of the *Chinese Journal of General Practitioners*. In 2018 and 2019, her abstracts were selected for poster presentation in IDF-WPR 2018 and IDF Congress 2019. Her research interest includes diabetes and its complications.

HUI ZHOU received the master's degree in endocrinology from Dalian Medical University, in June 2008. She worked as the Associate Chief Physician at the Department of Endocrinology, Sichuan Academy of Medical Sciences and Sichuan Provincial People's Hospital. Her research direction is diabetes and its complications.